Environmental Science Nano

Particle Dynamics of Nanoplastics Suspended in Water with Soil Microparticles: Insights from Small Angle Neutron Scattering (SANS) and Ultra-SANS

Journal:	*Environmental Science: Nano*
Manuscript ID	EN-ART-12-2024-001199.R2
Article Type:	Paper

Environmental Statement

Nanoplastics (NPs) occur in agroecosystems, originating from agricultural plastics such as mulch films, and can reside in the soil for several months or years. Even if derived from biodegradable plastics, they can serve as vectors for pesticides and other toxicants, potentially impacting soil biota and crops, threatening the food web, and promoting pollution to nearby waterways. Our results demonstrate that collisions between NPs and soil microparticles resulting from modest convection can reduce the size of NPs from 500-1100 nm to <50 nm, where they will be well dispersed in monomeric form, thereby enabling their transport in agroecosystems and increasing their ability to cross biological barriers and induce ecotoxicity.

Particle Dynamics of Nanoplastics Suspended in Water with Soil Microparticles: Insights from Small Angle Neutron Scattering (SANS) and Ultra-SANS

Journal: ***Environmental Science: Nano***

Anton Astner [a], Sai Venkatesh Pingali [b], Hugh O'Neill [b], Barbara Evans [b], Volker Urban [b], Kenneth Littrell [b], Douglas Hayes[a,*]

[a] The University of Tennessee, Biosystems Engineering and Soil Science, 2506 E J. Chapman Dr, Knoxville, TN 37996, United States of America

[b] Oak Ridge National Laboratory, 1 Bethel Valley Road, Oak Ridge, TN 37831, United States of America

*Corresponding author, e-mail: dhayes1@utk.edu

Abstract

Small-angle neutron scattering (SANS) and Ultra-SANS (USANS) were employed to understand the aggregation behavior and observe the size reduction for nanoplastics (NPs) formed from a biodegradable mulch film, and microparticles of vermiculite (V), an artificial soil, suspended in water in the presence of low convective shear (*ex-situ* stirring) prior to measurements. Neutron contrast matching was employed to minimize the signal of V (by 100-fold) and thereby isolate the signal due to NPs in the neutron beam, as the contrast match point (CMP) for V (67 vol% deuteration of water) differed from that of NPs by more than 20%. The original NPs' size distribution was bimodal: < 200 nm and 500-1200 nm, referred to as small and large NPs, i.e., SNPs and LNPs, respectively. In the absence of V, SNPs formed homoaggregates at higher concentrations that decreased with stirring time, while the size of LNPs remained unchanged. The presence of V at 2-fold lower concentration than NPs did not change the size of SNPs but reduced the size of LNPs by nearly 2-fold as stirring time increased. Because the size of SNPs and LNPs did not differ substantially between CMP and 100% D_2O solvents, it is evident that SNPs and LNPs are mainly composed of NPs and not V. The results suggest that LNPs are susceptible to size reduction through collisions with soil microparticles via convection, yielding SNPs near soil-water interfaces within vadose zones.

Keywords

Nanoplastics, nanoparticle dynamics, neutron contrast matching, small-angle neutron scattering, soil

1 INTRODUCTION

Plastic pollution is an emerging environmental concern for agroecosystems, particularly microplastics (MPs; 1 μm < particle diameter *(d_p)* < 5000 μm) and nanoplastics (NPs; d_p < 1000 nm), [1, 2]. MPs and NPs (M/NPs) are often harmful to soil biota, including earthworms, hexapods, microorganisms, and plants [3-10] and can harm biodiversity [11, 12]. M/NPs can serve as vectors for microorganisms that may carry genes for pathogens, pesticides, heavy metals, and other toxicants due to their hydrophobic nature [13, 14]. M/NPs can severely impact soil properties such as water retention characteristics, hydraulic conductivity, nutrient cycling processes [15, 16]. In addition, agricultural soils serve as a reservoir for MPs, allowing for their transport into adjacent waterways via runoff or groundwater recharge [9, 17, 18], potentially harming fish, bivalves, microalgae, and crustaceans and producing long-term toxicological effects in marine and freshwater organisms [19-21]. Even biodegradable M/NPs, originating from biodegradable mulch films after their incorporation into the soil [22-24], may require several months or years to fully biodegrade [25].

NPs present a greater threat to agroecosystems than MPs because of their smaller size, allowing them to penetrate biological barriers such as cell walls, producing a greater surface area exposure to biota, and increased colloidal stability in water [26]. NPs in agricultural soils can enter plant tissues through the roots [27], stems and leaves [28, 29], therefore threatening the safety of food supplies because of NPs' potential toxicity to humans [30-32]. The high mobility of NPs allows them to readily undergo transport in the vadose zone: horizontally between soils and nearby streams and lakes and vertically from soil into groundwater. Their smaller size makes their isolation and detection difficult to achieve. Analysis in environmental systems, particularly soil, typically involves several isolation and purification steps to enable characterization and quantification of NPs, e.g., via scanning electron microscopy (SEM), transmission electron microscopy (TEM), and pyrolysis gas chromatography-mass spectrometry (GC-MS) [33-35]. Alternatively, dynamic light scattering (DLS) can be employed to measure particle size of NPs and their homoaggregates under idealized laboratory conditions [36-38]. The dynamics of NPs in agroecosystems are not fully understood. In water, polystyrene (PS)-NPs are likely to undergo homoaggregation in the presence of increased ionic strength (e.g., at concentrations similar to seawater), multivalent cations, lower temperature, and higher salinity, while the presence of humic acid and other forms of natural organic matter (NOM) reduce aggregation [36, 39]. Moreover, while ionic strength reduces the magnitude of the zeta potential by Debye shielding, NOM reduces the shielding

through steric repulsion [40]. In freshwater and groundwater, NPs are less likely to aggregate unless they adsorb significant amounts of dissolved NOM [37].

The fate and transport of NPs in agroecosystems is strongly influenced by their behavior near water-soil interfaces, where NPs will likely encounter dispersions of soil particles in streams and lakes, potentially leading to heteroaggregation, a topic that has only recently investigated. Heteroaggregation between soil and NPs is more likely to occur than homoaggregation of NPs [38, 41]. Heteroaggregation can significantly affect migration of NPs in surface waters, which may explain challenges in isolating NPs through flotation or soil leaching. PS-NPs aggregate with positively-charged soil minerals (e.g., hematite, goethite and magnetite under acidic and neutral pH) via electrostatic attractive interactions at low salinity (or equivalently, positively-charged NPs and negatively-charged minerals [42]), and to a much lesser extent for negatively-charged minerals (e.g., montmorillonite and kaolinite) or when the surface of positively-charged NPs is neutralized by NOM [41, 43, 44]. Heteroaggregation frequently corresponds to a zeta potential near zero [41, 43, 44]. In agreement, another report describes insignificant heteroaggregation between PS-NPs and negatively-charged minerals [43]; but, heteroaggregation was observed in the presence of NOM, which decreased the strength of van der Waals attractive forces [36, 38].

The structure of NP-soil heteroaggregates, important for understanding and predicting the transport behavior in water-soil systems and environmental stability, is not well understood. Soil components, like NOM and minerals, can interfere with detection when using microscopic or spectroscopic techniques [27]. DLS, employed in many of the studies cited above, provides an overall average size for aggregates (hydrodynamic radius) without providing detail on the structure, in terms of its composition and geometry and can be performed only on dilute concentrations of simple NP-mineral systems. SEM and TEM have been employed in a few instances [36, 43, 44]; however, microscopy requires preparation methods that can introduce artifacts and micrographs from one subsample may not be reflective of structure across the entire system. Moreover, microscopy cannot be used *in situ*.

We recently presented the proof-of-concept for using Small Angle Neutron Scattering (SANS) and Ultra-SANS (USANS) to achieve this purpose [45]. Our previous study involved suspensions of NPs prepared from BDMs and microparticles of vermiculite (V), a mineral of clay, in partially deuterated water. V was chosen as a surrogate soil due to its silt-like characteristics, efficient water dispersion, and high monodispersity, which aided in interpretation of SANS data. Unlike microscopic techniques, SANS allows for *in situ* nanoscale measurements of size, geometry, and kinetics of NPs and other colloidal media in real time. Neutrons are a non-destructive probe and are highly sensitive to isotopic

differences. For example, normal water has a neutron scattering length density of -0.56x10^{-6}Å^{-2} while fully deuterated water has a scattering length density of 6.35 x10^{-6}Å^{-2}, with most materials having scattering length densities between these values; the effect of substituting deuterium (^{2}H) for normal hydrogen (^{1}H) in other hydrogenous compounds is similar, albeit usually less dramatic. This allows the use of selective deuteration of solvents and/or other system components to mask or highlight different parts of a system by contrast variation and—when the scattering length densities of the solvent and a particular component are the same, making it disappear from the scattering— neutron contrast matching.

We employed the contrast matching technique in our previous study for NPs to be isolated from a mixture of NPs in vermiculite sample in the neutron beam [45]. A SANS contrast variation study, scattering intensity vs. deuteration level in water, for suspensions of V found that 67% deuteration of the water was optimal for minimizing the scattered intensity of V; 67% D_2O / 33% H_2O serves as the contrast match point (CMP) for V. Operation at the CMP did not completely eliminate the signal for V but reduced its signal 50-100 -fold relative to using 100% D_2O. We found that NPs and their aggregates produced oscillations in the SANS data that were fit using form factor models, thereby providing information on size and shape. We investigated NPs in the absence and presence of V suspended in CMP solvent, with suspensions analyzed either immediately after formation or after undergoing *ex-situ* stirring for 24 h. Results demonstrated that for NPs of particle diameter (d_p) > 200 nm, both the presence of V and stirring reduced the volume fraction and size of detected NPs, presumably due to the formation of larger aggregates that are too large to view via SANS, while smaller-sized (~50 nm) NPs did not undergo any significant changes in size or concentration.

The objective of the current study, an expansion of the preliminary study, is to investigate the impact of convection (*ex-situ* stirring time), NP concentration, and the presence and absence of soil microparticles on the aggregation behavior of and dimensional properties of NPs in water, as would be encountered in the vadose zone of agroecosystems [46]. In addition to CMP solvent, 100% D_2O was used as solvent for a series of equivalent samples to help differentiate between homoaggregation and heteroaggregation of NPs and the small population of nanoscopic V particles that form. A deeper understanding is essential for predicting the long-term fate, transport, and biodegradability of terrestrial NPs, particularly at water-soil interfaces, as needed to provide critical insights for risk assessments and remediation strategies.

Most of the studies of NP aggregation in the literature employ idealized monodisperse NPs (e.g., of PS) that hardly resemble NPs occurring in nature. Moreover, a recent study found that nonspherical

NPs underwent homoaggregation at a lower salinity than spherical NPs [47]. In addition, many of the NP standard materials contain surfactants resulting from the preparation procedure that cause artifacts in the observed aggregation behavior observed [26]. Therefore, both the previous and current SANS studies have employed polydisperse NPs derived from BDMs that likely mimic NPs occurring in nature. Moreover, knowledge of aggregation for biodegradable NPs has been understudied.

2 MATERIALS AND METHODS

2.1 Materials

NPs were prepared from a roll of pristine BioAgri (Biobag Americas, Palm Harbor, FL, USA), a BDM film composed of Mater-Bi® resin (grade EF04P; Novamont, Novara, Italy), which consists of a PBAT/starch blend. BioAgri possessed an apparent density of 22.81 ±0.41 g m^{-2} and a thickness of 29 ±1.2 μm [48, 49]. Other properties of BioAgri are provided in the cited references. NPs were prepared according to our published procedure [50]. BioAgri film (15 g; 0.5 m^2) was treated with a mixture of water and liquid nitrogen under shear using a blender and was subsequently milled to form MPs and then sieved into various fractions. NPs were formed by subjecting the 106 μm MP size fraction to a highly efficient wet grinding process employing 60 passes. According to the particle size analysis through DLS, the produced PBAT NPs possess a bimodal size distribution, with the distribution of each subpopulation described by a lognormal distribution, with the maximum d_p values for the subpopulations occurring at 51 nm and 122 nm and d_p ranging between 33 and 955 nm. The average d_p value was 131.7 nm [51]. An atomic force microscopic (AFM) image of the NPs, provided in **Fig. S1A**, is consistent with the findings. Vermiculite ($Mg_{1.8}Fe^{2+}_{0.9}Al_{4.3}SiO_{10}(OH)_2 \cdot 4H_2O$) (V), grade 4, mesh size 7.9 mm, was purchased from Uline (Pleasant Prairie, WI, USA). The raw particles averaged 4.65 ±2.39 mm in size, whereas the length-to-width (L/W) ratio was 1.39 according to ImageJ [52] software. The larger particles were mechanically ground with a mortar and pestle grinder and sieved through meshes of 840 μm, 250 μm, 106 μm, and 45 μm. The latter sieve fraction was employed in the SANS and USANS experiments. The particle density of V was 2.4 g/cm^3, and the average particle size assessed using an Olympus SZ 61 stereomicroscope (Shinjuku; Tokyo, Japan) and a Nikon Digital Sight DS-Fi1 camera (Shinagawa; Tokyo, Japan) and ImageJ software, was 38 ±12 μm (i.e., monodisperse), based on analysis of 250 particles. This size range corresponds to medium silt [53], the

most prominent soil type found near soil-freshwater interfaces [54, 55]. Deuterium oxide (D_2O; 99.99% pure) was purchased from Acros (Geel, Belgium). Deionized water was employed throughout.

2.2 Methods

2.2.1 Preparation of aqueous suspensions of NPs and V

Separate suspensions of NPs and V in either 100% D_2O or a mixture of 67% (vol) D_2O and 33% H_2O were prepared in 7 mL borosilicate glass scintillation vials and served as stock solutions. The latter solvent was previously identified as the CMP for V [45]. Sample mixtures were prepared by mixing appropriate volumes of NP and V stock solutions, resulting in overall concentrations of 0.5% (i.e., 5000 ppm or mg/L) for V and 1% (10,000 ppm) or 5% (50,000 ppm) for NPs. NP concentrations, although higher than used in most colloidal stability studies and reported in environmental studies (1-100 ppm) [56, 57], were chosen to better observe any long-term interactions between NPs and V that would occur, to mimic the higher NP concentration that may occur near soil-water interfaces when exposed to convection, and to ensure resolution by SANS. Samples were magnetically stirred (*ex-situ*) at a rate of 400 min^{-1} for either 0 h, 24 h, or 168 h at room temperature (22±1°C). Samples corresponding to 0 h of stir time were stirred for a short (30 min) duration and then were allowed to settle for over 12 h for proton exchanges and water (D_2O) penetration into pores to reduce the incoherent background scattering. Before SANS and USANS experiments, all sample suspensions were briefly vortexed and transferred with a syringe into titanium tumbler cells with a 1.0 mm path length (0.4 mL volume). The cells were positioned in sample holders designed for the SANS and USANS instruments and gently tumbled at a selected rotation speed of 10 min^{-1} that allowed all suspended particles to be exposed to the neutron beam.

To determine the fraction of NPs and V that would remain suspended in solution for a long time, batch tests were performed on replicate samples of those analyzed by SANS and USANS, with microcentrifugation at 12,000 rpm and room temperature for 10 min performed. Supernatant was separated from particles that settled out after centrifugation through micropipetting. The remaining particles were dried at 105°C overnight and weighed, with the fraction of particles suspended calculated via a mass balance.

2.2.2 Small angle neutron scattering (SANS) and ultra-SANS (USANS) measurements

SANS measurements were performed using the Bio-SANS and USANS 1A beamlines at the High Flux Isotope Reactor (HFIR) and Spallation Neutron Source (SNS) facilities at Oak Ridge National

Laboratory (ORNL), Oak Ridge, TN USA, respectively. Additional details on the instrumentation are provided elsewhere [58-60].

For SANS data collection, an extensive dynamic Q range was investigated, spanning from 0.003 to 0.8 Å^{-1} in a single configurational setting using neutrons at a wavelength (λ) of 6.09 Å and a relative wavelength spread ($\Delta \lambda/\lambda$) of 15%. The main detector was located 15.5 m from the spectrometer, and the wing detector array was fixed at 1.13 m from the spectrometer at an angle of 1.4°, allowing for the collection of the momentum transfer (Q), defined as follows:

$$Q = 4 \pi \lambda^{-1} \sin(\theta/2) \quad (1)$$

where θ is the scattering angle.

USANS measurements were performed at a sample-to-detector distance of 30 m on a time-of-flight triple-bounce Bonse–Hart small-angle scattering spectrometer. Neutron wavelengths of 0.9, 1.8, and 3.6 Å were separated from the primary beam by time-of-flight and used to access a Q-range of 5 x 10^{-5} - 2 x 10^{-3} Å^{-1}.

The beam exposure times of the samples were at 0.5 - 2.5 h and 8 - 12 h for SANS and USANS, respectively. Error bars for $I(Q)$ result from counting statistics. Data reduction of SANS and USANS data (scattered intensity $I(Q)$ vs. Q) was performed using a Python® script written and developed by ORNL. SANS and USANS intensities were adjusted for empty cell and solvent scattering and beam background, and the SANS instrument was calibrated to an absolute scale using a Porasil silica standard. USANS data underwent slit-desmearing considering a slit height of 0.042 Å^{-1} (in units of momentum transfer) using the Igor Pro USANS package developed by scientists at the National Institute of Standards Center for Neutron Research (NIST-NCNR) [61] to correct the instrumental resolution effects inherent in the finite collimation and detector geometry. The slit-desmearing process involved modeling the instrument's resolution function, which characterized the smearing effect as a convolution of the true scattering intensity. The resolution function was determined through calibration measurements and implemented using iterative deconvolution techniques, represented by the Richardson-Lucy algorithm. After merging the SANS and USANS curves, data fitting and data distribution analysis were conducted using the 'Modeling-II' tool in the IRENA [62] package of Igor Pro (WaveMetrics, Inc., Lake Oswego, OR) software. The combined USANS and SANS data were analyzed with a unified structural model across the entire wavevector range.

2.2.3 SANS and USANS data analysis

SANS and USANS datasets were merged through alignment to the power law function for the Porod region, for which $1/2\ Q\ d_p >> 1$ [59]:

$$I(Q) = \alpha Q^{-\beta} + I_{bkg} \quad (2)$$

where α, β, and I_{bkg} represent the intensity scale factor, the power law exponent, and background intensity, respectively. To obtain the surface fractal, D_s, the simple formula $D_s=6-\beta$ was employed [63]. Values 3 and 4 for β (i.e., D_s = 3 and 2, respectively) represent rough and smooth surfaces, respectively. The generated power law (**Eq. 2)** that provided the best fit to the data was subtracted from the merged SANS and USANS dataset**,** and the resultant data $(I(Q)-\alpha Q^{-\beta})$ represent oscillations due to suspended NPs that occurred at low- and high-Q that were fitted using form factor ($P(Q)$)-structure factor ($S(Q)$) modeling. Finally, the high-Q region (linear portions) of the combined SANS and USANS curves (after subtraction of **Eq. 2**) was modeled to the power law function in the "Unified Fit" and "Modeling II" functions [62].

The $P(Q)$ model used for oscillations for the high-Q region (0.003-0.5 Å^{-1}) was a *lognormal spherical* radial distribution of polydisperse spheres provided by the IRENA package:

$$I(Q) = I_0\, exp\left(-\frac{(\,ln(Q) - ln\,(\mu))^2}{2\sigma^2}\right) \quad (3)$$

where I_0 is the scale factor; (σ) is the standard deviation of particle size (radius R) on a log scale and represents the polydispersity of particle size; μ is the mean value; $\mu = ln\,(R_{med})$, where R_{med} is the median radius.

The $P(Q)$ model providing the best fit for oscillations occurring in the low-Q region, collected by USANS (5x10^{-5} – 2x10^{-3}, Å^{-1}), was *polydisperse spheres with a Schulz distribution* for the radius [64, 65]. The (normalized) **Schulz distribution** is described as follows:

$$I(Q) = I_0\left(1 + \frac{Q^2\, R_g^2}{3}\right)^{-\frac{v+1}{2}} \quad (4)$$

where R_g is the radius of gyration and v is the polydispersity index, termed *pd*. The average radius, R, i.e., $0.5d_p$, is calculated by multiplying R_g by the square root of 5/3. I_0 for spheres is defined as follows:

$$I_0 = \phi \cdot (\Delta\rho)^2 \cdot \frac{4}{3}\pi R^3 \quad (5)$$

where ϕ is the volume fraction of the particles, and $\Delta\rho$ is the difference in scattering length density between NPs and the solvent. Values of ρ for 100% D_2O, CMP solvent (67 vol % D_2O and 33 % H_2O mixture), and PBAT-NPs are (×10^{-6} Å^{-2}) 6.35, 4.08, and 0.99, respectively. $S(Q)$ models consisted either of 1.0 (dilute solutions) or *interferences*, for which particles show spatial correlations or ordering [66].

The collected size distribution data were used to generate histograms and box plots. In addition, the particle size distributions for both Schultz spheres and lognormal models were statistically evaluated by analysis of variance (ANOVA). In contrast, small *p*-values of less than 0.05 were considered statistically significant.

3 RESULTS

Our previous SANS/USANS study demonstrated that convection time (0 h vs. 24 h) changed the size and aggregation behavior of NPs dispersed in water at 1 wt% in the presence and absence of soil (V) microparticles (0.5%) [45]. To gain a deeper insight into particle dynamics changes, the set of conditions for this study was extended by increasing the convection time to 1 week (168 h) and employing an additional NP concentration, 5 %, and an additional solvent, 100 % D_2O. The latter solvent enables the combined scattering from NPs and V particles of size < 1000 nm to be observed. The fitting approach, i.e., *P(Q)S(Q)* model fitting of the oscillations after subtraction of a power law relationship representing Porod-scattering **(Eq. 2)** from the merged SANS and USANS data, as established in our previous study [45], provided information on the particles' geometry, size, size distribution, relative volume fractions, and aggregation behavior**.** A total of 18 SANS and USANS samples were evaluated, of which 9 samples each employed the CMP for V (67% D_2O/33% H_2O) and 100% D_2O as solvent.

3.1. Impact of *ex-situ* stirring time and solvent on fraction of NPs and V that remain suspended in solution (batch tests)

Batch tests were conducted to determine the concentration of NPs and V that would remain suspended in solution after stirring was stopped for the NP and V concentrations and stirring time, and for both D_2O and CMP solvents. The particles remaining in solution are likely the particles contributing to the oscillations in the SANS and USANS data since particles settling out of suspension would likely not be undergoing Brownian motion. Under all conditions, only 3-13% of NPs + V remained suspended; the majority settled out **(Fig. 1)**. We analyzed both fractions formed from 1% NPs suspended in CMP solvent via AFM and found a selectivity toward smaller d_p values for the suspended particles compared to NPs that settled out **(Fig. S1)**. For both solvents, the concentration of V that remained suspended decreased with stirring time, indicating the propensity of V microparticles and homoaggregates to settle out of solution. In contrast, the concentration of suspended NPs (in the absence of V) increased with stirring time, suggesting that stirring decreased NP homoaggregation

and/or induced size reduction. The CMP solvent produced lower concentrations of suspended NPs and V compared to 100% D_2O. For NPs+V at both 5% and 1% NP concentrations, the concentration of particles suspended in water also increased with stirring time and was higher in D_2O than in CMP solvent, with the exception of 5% NP+V, for which the mass of suspended particles was smaller in 100% D_2O **(Fig. 1)**.

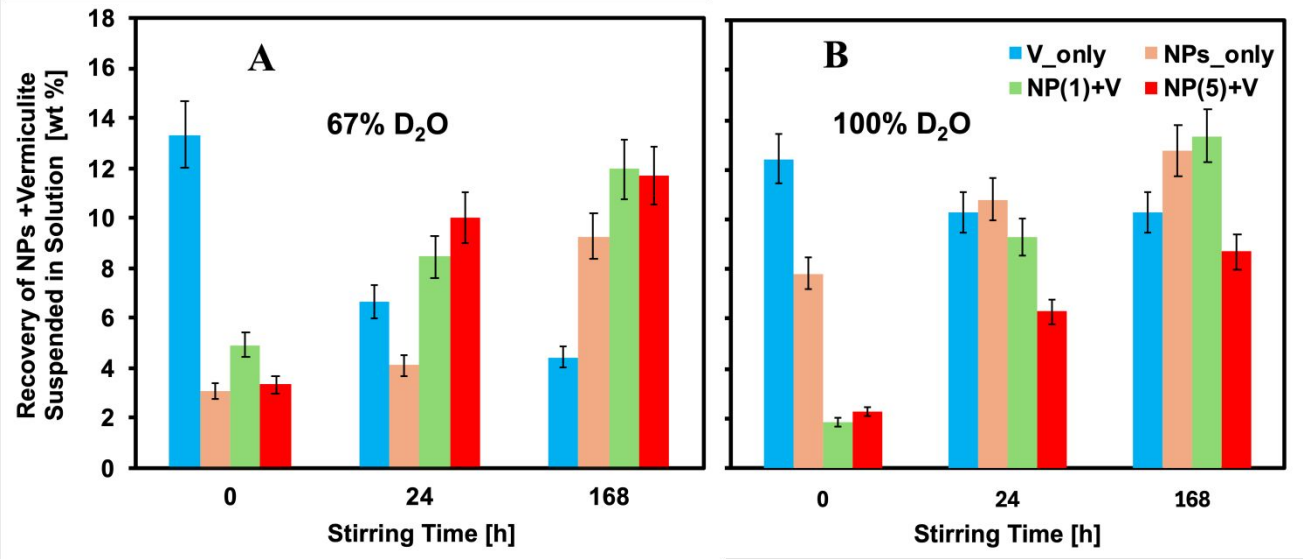

Fig. 1 Recovery yield (%) of vermiculite (V_only), nanoplastics (NPs_only), and their mixture in metastable suspensions (1% and 5% NP+V) after centrifugation for **(A)** CMP and **(B)** 100% D_2O solvents at various *ex-situ stirring* times (0, 24, 168 hours). Error bars represent the standard error of the measurements.

3.2. Impact of *ex-situ* stirring time on fractal dimensions for NPs and V

Figs. S2-S4 display the effect of convection (*ex-situ* stirring) on the combined SANS/USANS data of a suspension containing NPs (1% or 5%) and/or V (0.5%) in both 67 vol% D_2O/33% H_2O (CMP solvent) and 100% D_2O, covering a range of length scales between 1 nm and 5000 nm. The signal observed for V alone can be attributed to the limited formation of nanoscale V particles (**Fig. S2**). Interestingly, in the presence of 100% D_2O, the scattered intensity of V alone increased slightly with an increase of stirring time, indicating that convective forces somewhat elevated the concentration of nanoscale V particles (**Fig. S2B**). The differing trends for V (nanoparticles) with increased stirring time across various solvents suggest distinct dispersion behaviors. In suspensions containing either 1% NPs or 1% or 5% NPs +V, the effect of convective stirring on the scattering levels was comparatively minimal (**see Figs. S2-S4).**

From observation of **Fig. S2**, it is apparent that contrast matching decreased the scattering attributable to V by an order of magnitude compared to 100% D_2O, demonstrating the effectiveness of

contrast matching. Moreover, for NPs (1%) +V, a slightly higher *I(Q)* level was observed in 100% D_2O than for the CMP solvent, suggesting the more prominent contribution of V toward scattering for the former solvent. However, contrast matching was not fully effective in removing V's signal, likely because of the heterogeneity in composition and particle density, hence in scattering length density, between V particles.

The Porod power law **(Eq. 2)** fit the SANS data well for all samples analyzed **(Figs. 2, S5, and S6)**. Values of β for NPs in the presence and absence of V, both solvents, and all stirring times were near 3.3-3.5 (D_s=2.5-2.7), as shown in **Table S1**, in agreement with our previous report [45], indicating a rough surface fractal, hence a rough surface for the pores of the NPs over the length scale being probed by SANS and USANS: 10 nm – 10 μm, consistent with the nonspherical geometry we observed for NPs [45]. The scattering of V alone exhibited a similar D_s as NPs in D_2O (2.67±0.03); but, a larger value of D_s was obtained in the presence of contrast matching (2.91±0.025), suggesting increased surface roughness. This result reflects the ability to see deeper solvent penetration into the pores of the V particles under contrast-matching conditions. It is apparent from the figures that oscillations occurred in both the low- and high-*Q* regions for NPs (8.5×10^{-5} Å$^{-1} \leq Q \leq 2 \times 10^{-2}$ Å^{-1} and 3.0×10^{-3} Å$^{-1} \leq Q \leq 3.0 \times 10^{-1}$ Å^{-1}, respectively), as we observed previously [45]. The oscillations, representing NPs and their aggregates, will be referred to as large NPs (LNPs) and small NPs (SNPs), respectively. In addition, a few samples produced oscillations at the low-*Q* range of USANS (5.7×10 Å$^{-5} \leq Q \leq 1.5 \times 10^{-4}$ Å^{-1}), to be referred to as small MPs (SMPs) since their size is above 1000 nm. The oscillations were very apparent once the Porod power law was subtracted; however, oscillations did not occur for V alone under all stirring and solvent conditions **(Figs. 3 and S7)**.

3.3. Aggregation behavior of NPs suspended in 67% D_2O/33% H_2O

Several different *P(Q)* models were applied to the oscillations in the SANS data. The models that provided the best fit for SNPs and LNPs were the lognormal **(Eq. 3)** and polydisperse spheres / Schultz distribution **(Eq. 4)** models, respectively. The model fits are represented in **Figs. 3 and S7** for the CMP and 100% D_2O samples, respectively, while parameters derived from the model fits are given in **Table 1**. The models provided the average size (d_p) and the size distribution, which are depicted via box plots, and histograms in **Figs. 4** and **S8**, respectively. The results for model fitting of CMP samples are described in this subsection.

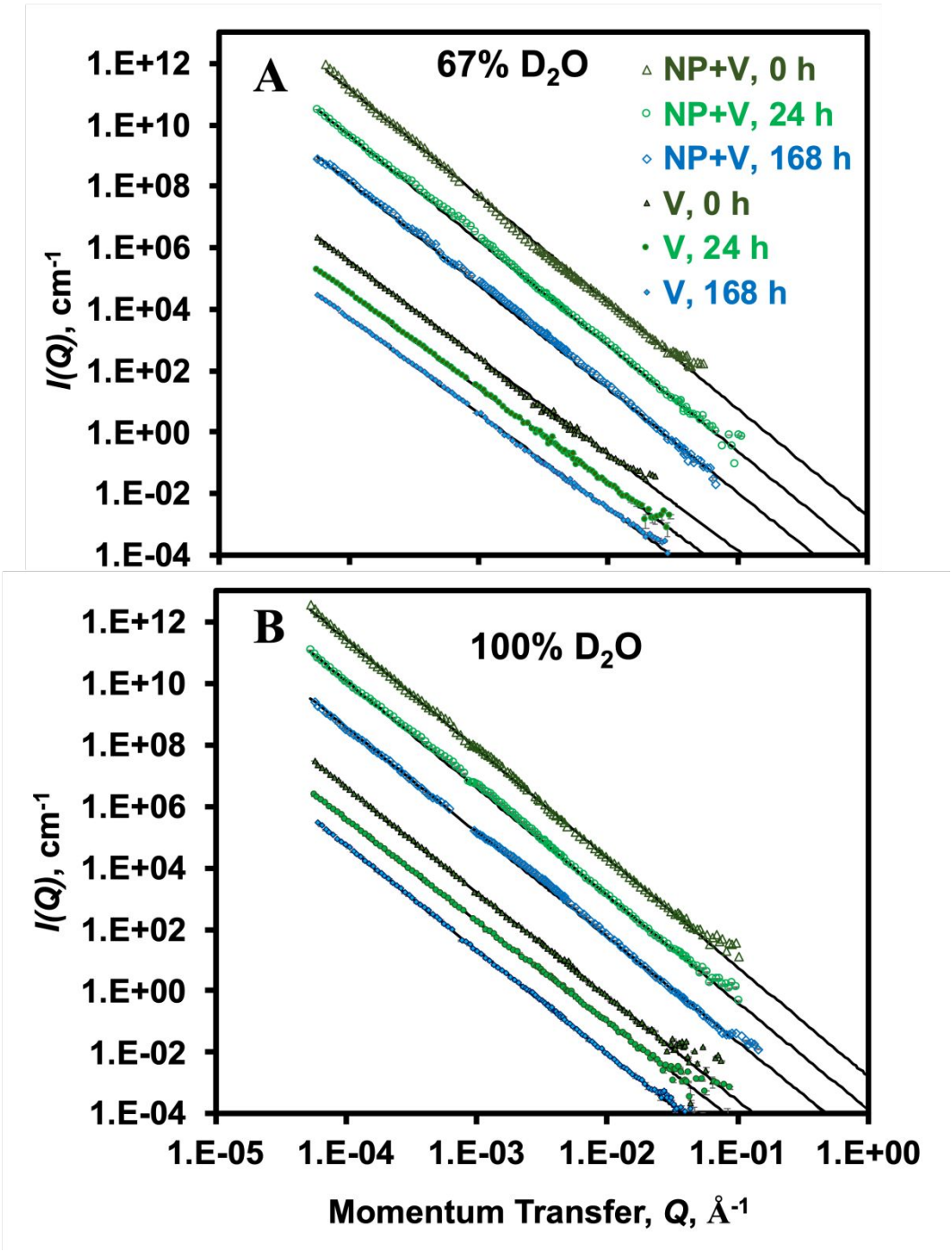

Fig. 2 Fitting of Porod power law relationship (Eq. 2) to the merged SANS and USANS data depicted in **Fig. S2** for suspensions formed by 1 wt. % and 0.5% PBAT NPs and vermiculite (V), respectively, in **(A)** 67 vol% D_2O/33% H_2O (contrast match point of V) and **(B)** 100% D_2O at 22°C and different *ex-situ* stirring times. For improved visualization in both **Figs. (A)** and (**B**), *I(Q)* data at 0 h, 24 h, and 168 h were multiplied by 5000, 250, and 10 for NP+V and by 1, 0.1 and 0.01, respectively, for V.

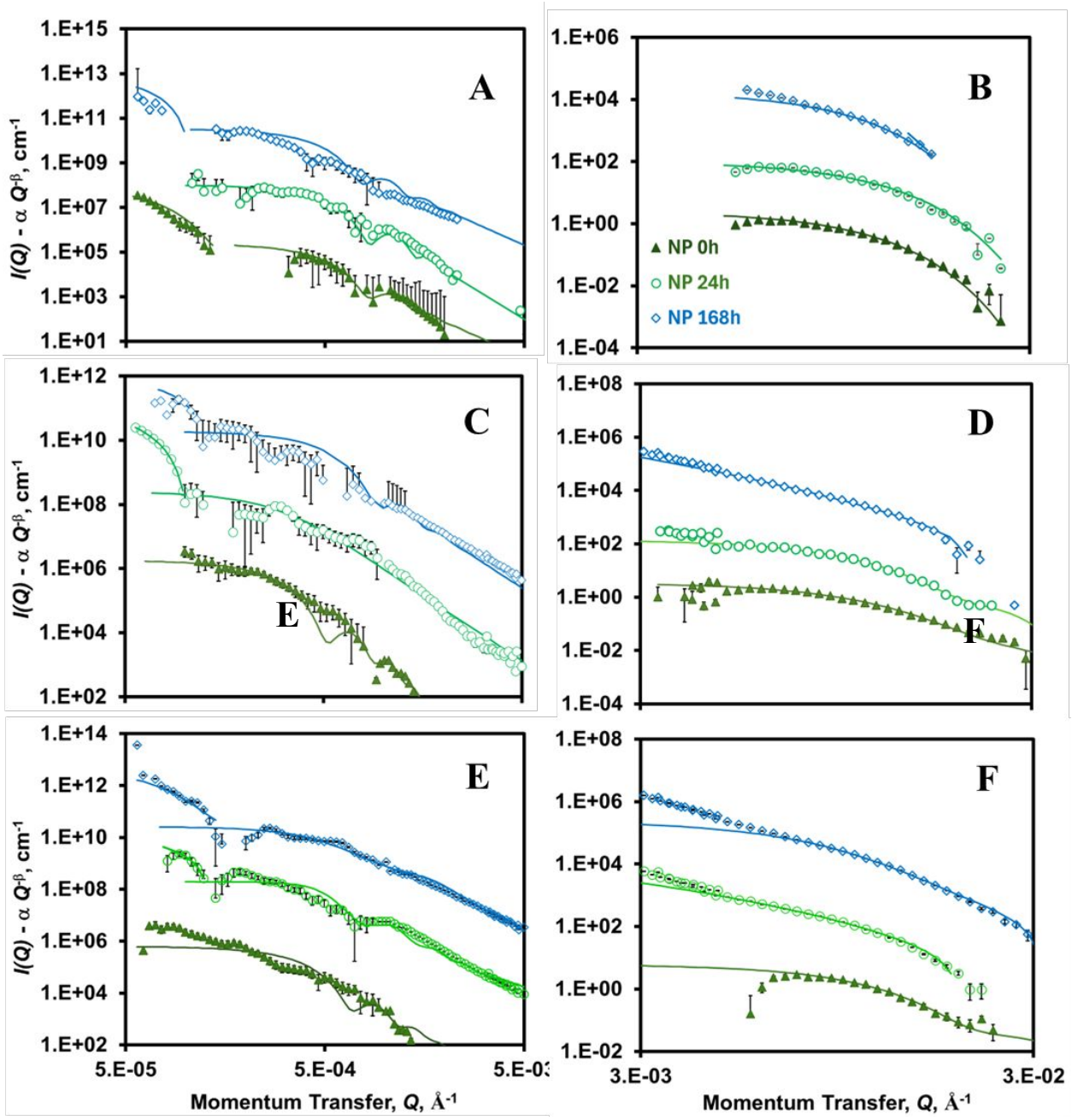

Fig. 3 Model fitting of oscillations for SANS and USANS scattering data after subtraction of the power law **(Eq. 2)** from *I(Q)* **(Figs. 2A, S5A, and S6A)** for suspensions of **(A, B)** NPs (1 %); **(C, D)** NPs (1%) + V (0.5%), and **(E, F)** NPs (5%) + V (0.5%) in contrast matching solvent for V (67% D_2O / 33% H_2O) at 22°C. **(A, C, E)** USANS data fitted by a Schulz polydisperse sphere form factor model (**Eq. 4)** for large NPs (LNPs) and **(B, D, F)** SANS data fitted by a lognormal form factor model (**Eq. 3)** for small NPs (SNPs). Parameters derived from the model fitting and structure factors are presented in **Table 1**. Data for **Figs. A, C, and E** were multiplied by factors of 500 (24 h), and 50,000 (168 h), and for **Figs. B, D, and F** by factors of 50 (24 h) and 5,000 (168 h), respectively, to improve visualization.

The employment of the CMP allowed for the direct detection of individual NPs and their presence in aggregates. In the absence of V, an increase in stir time led to a slight decrease of d_p and a narrower

size distribution for SNPs, with d_p remaining near 50 nm, while the average size of LNPs and SMPs remained near 1200 nm and 6000 nm, respectively, with the size distribution broadening between 24 and 168 h of stir time. Moreover, convection did not appear to induce homoaggregation. Analysis of the same PBAT NPs dispersed in H_2O (0 h *ex-situ* stirring) by DLS also produced a similar bimodal size distribution for NPs, with the average size of SNPs and LNPs being 51 nm and 200 nm [51]. The difference in size range for LNPs between methods may result from the use of centrifugation during the sample preparation for DLS and the lower density of H_2O relative to D_2O, both of which may induce larger NPs to settle out **(Sect. 4.5)**. Moreover, the sample preparation method employed for analysis of NP size (e.g., via SEM, TEM, or DLS) may introduce artifacts; in contrast, SANS/USANS serves as an *in situ* method for analysis of size, size distribution, and geometry. As stir time increased, ϕ for SNPs increased while ϕ for LNP did not change appreciably (within error), possibly indicating the size reduction of LNPs into SNPs **(Table 1)**.

For NPs (1%) in the presence of V, the size of SNPs decreased slightly, by ~8 nm, when subjected to 168 h stirring. An ANOVA indicated no significant difference for d_p of SNPs (1%) in the absence vs. presence of V ($p < 0.09$). Values of ϕ decreased with stir time for SNPs and were smaller than corresponding ϕ values in the absence of V, indicating that SNPs form large heteroaggregates with V microparticles that are outside the size range for USANS **(Table 1)**. In contrast, LNPs underwent an approximately 50% decrease of d_p, by 440 nm ($p < 0.001$) **(Fig. 4)**. Even the employment of ~30 min of stirring (for "0 h" treatment) in the presence of V led to a slight decrease in d_p for LNPs **(Fig. 4)**. Also, the size distribution of SNPs and LNPs narrowed as the *ex-situ* stirring time increased **(Figs. 4 and S8).** These observations suggest that LNPs are more susceptible to size reduction than SNPs in the presence of convection due to collisions with V microparticles. Similarly, our study of the effect of shear from wet grinding on NPs indicated a decrease in size for the population of LNPs with increasing exposure time [51].

For NPs at a higher concentration, 5%, in the presence of V, representing a 1.5-fold higher NP/V ratio than for 1% NP, SNPs possessed a larger particle size than for the samples containing 1% NPs, but with the size decreasing to 50 nm upon stirring, the same d_p value observed for 1% NPs **(Fig. 4A)**. This observation suggests that at higher concentrations, SNPs form mainly homoaggregates that are readily broken up by convective shear. Mirroring the trend observed for 1% NPs in the absence of V, the size of LNPs remained constant with stirring time between 0 and 24 h but with a slight decrease of size from 24 h to 168 h **(Fig. 4B)**. The average size of LNPs for 5% NP+V was slightly smaller than that for 1% NPs in the absence of V, suggesting that V induced size reduction for LNPs **(Fig. 4C).**

The comparison of size distribution data for 5% and 1% NPs in the presence of V allows one to differentiate between the size reduction of NPs and the breakup of NP aggregates. In the absence of convective stirring, the sharing of a common d_p for LNPs, despite a 5-fold difference in NP concentration, suggests the observed LNPs are likely single particles rather than NP aggregates, and the observed size reduction of d_p for LNPs with stir time for 1% NPs represents an actual reduction in size rather than the breakup of aggregates. In contrast, the larger size for SNPs at 5% compared to 1% NP concentration likely represents homoaggregation, and the decrease of d_p with stir time for 5% NP likely represents the breakup of aggregates. The slight decrease of d_p for NPs at 1% concentration with increased *ex-situ* stirring time occurred at the high end of the size distribution for SNPs, suggesting that size reduction selectively occurs for larger-sized SNPs **(Figs. 4A and S8A)**.

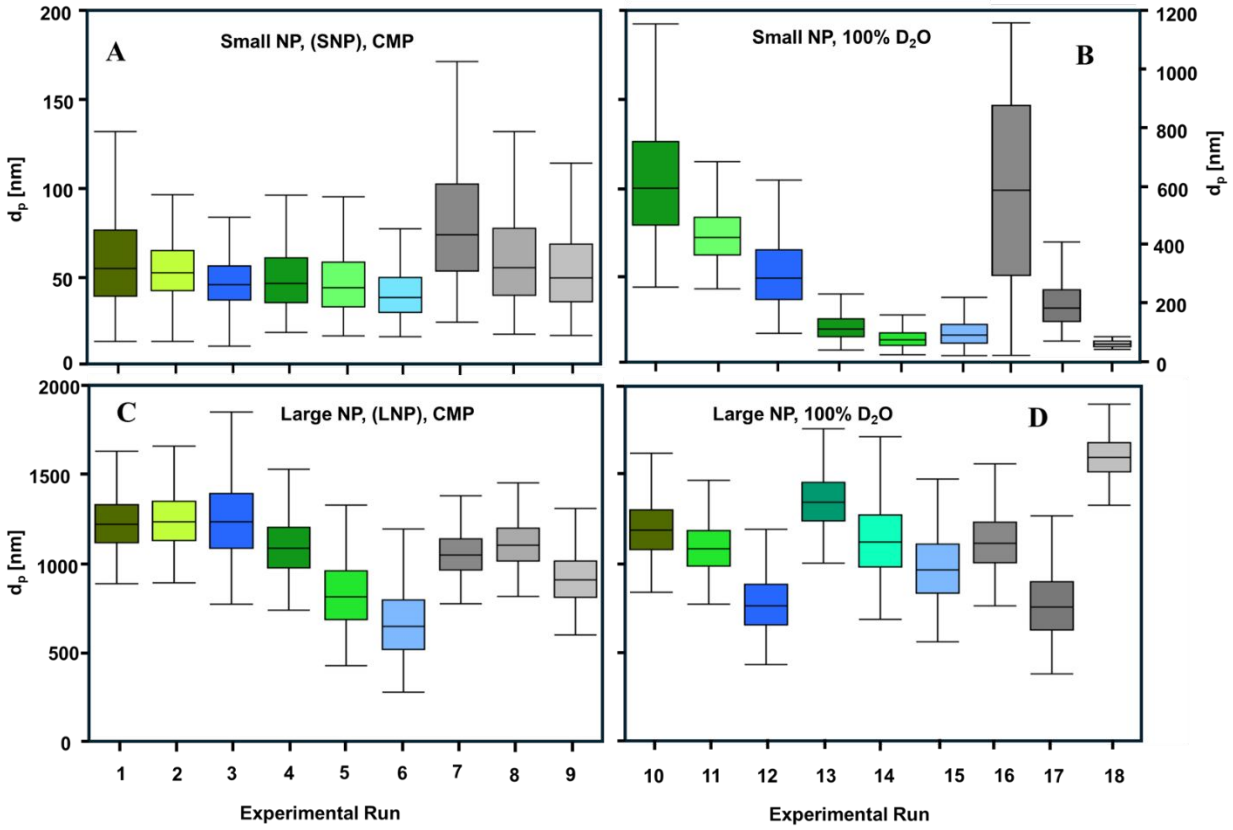

Fig. 4. Box plots for size (d_p) of NPs or their aggregates suspended in aqueous suspensions at the CMP of V (67 vol% D_2O/33% H_2O): **(A)** SNPs and **(B)** LNPs vs. *ex-situ* stirring time and NP and V concentrations and NPs or their aggregates suspended in 100% D_2O: **(C)** SNPs and **(D)** LNPs vs. *ex-situ* stirring time and NP and V concentration. Experimental Runs refer to "Samples" as defined in **Table 1.** Secondary y-axis for **Fig. B** corresponds to Runs 16-18.

Table 1. Model fitting Parameter values derived from the Lognormal and Schultz form factor models applied SANS and USANS data, respectively, after subtraction of the power law relationship, for suspensions of NP and V in water, [1-2]

Composition	**NP [1%]**			**NP [1%] +V [0.05%]**			**NP [5%] +V [0.05%]**		
Sample #	**1**	**2**	**3**	**4**	**5**	**6**	**7**	**8**	**9**
***Ex-situ* stirring time [h]**	**0**	**24**	**168**	**0**	**24**	**168**	**0**	**24**	**168**
I. D_2O/H_2O 67/33 v/v (Contrast Match Point, CMP)									
A. Small NPs, SNP (SANS; lognormal model)									
FW-HM [3]	37	31	30	42	32	24	35	33	29
Upper 95% Mean [nm]	49.6	55.9	48.3	51.1	48.9	41.7	86.4	64.9	57.3
Lower 95% Mean [nm]	43.2	50.4	43.6	44.8	42.5	36.8	73.8	55.0	48.9
Volume Fraction, ϕ x10^4	0.48±0.02	0.58±0.03	0.81±0.05	0.40±0.03	0.35±0.04	0.15±0.02	0.62±0.06	0.57±0.07	0.36±0.04
B. Large NPs, LNPs (USANS; polydisperse spheres with a Schultz Distribution)									
FW-HM [3]	351	361	498	373	438	429	277	301	332
Upper 95% Mean [nm]	1241	1258	1274	1110	852	690	1064	1120	930
Lower 95% Mean [nm]	1192	1207	1203	1058	789	626	1024	1078	883
Coefficient of Variation	13%	13%	18%	15%	21%	30%	12%	12%	16%
Polydispersity, pd	0.107	0.085	0.118	0.089	0.372	0.229	0.124	0.110	0.185
Volume Fraction, ϕ x10^4	4.71±1.7	6.72±1.1	5.68±1.2	8.22±2.2	8.12±2.9	12.2±2.1	1.6±0.3	7.6±1.7	8.7±1.9
C. Small Microplastics, SMPs (USANS; polydisperse spheres with a Schultz Distribution)									
FW-HM [3]	2898 [4]	N/A [5]	2397 [4]	N/A	2861	6928	N/A	2675 [4)]	2867 [4)]
Upper 95% Mean [nm]	8701	N/A	6686	N/A	7986	8325	N/A	6779	5262
Lower 95% Mean [nm]	8356	N/A	6312	N/A	7982	6782	N/A	6778	4997
Coefficient of Variation	2%	N/A	2%	N/A	1%	1%	N/A	1%	1%
Sample #	**10**	**11**	**12**	**13**	**14**	**15**	**16**	**17**	**18**
II. 100% D_2O									
A. Small NPs, SNP (SANS; lognormal model)									
FW-HM [3]	83	43	36	42	11	12	85	37	26
Upper 95% Mean [nm]	111	76.7	57.5	51.1	17.2	21.1	606	196	51.2

Lower 95% Mean [nm]	100.0	71.7	50.5	44.8	15.5	18.4	501.8	168.7	45.0
Coefficient of Variation	33%	21%	15%	45%	36%	28%	51%	46%	32%
Volume Fraction, ϕ x10^4	5.5±0.7	3.9±0.5	3.1±0.6	8.5±0.9	3.5±0.7	4.6±0.8	8.1±0.7	5.7±0.5	3.5±0.1
B. Large NPs, LNPs (USANS; polydisperse spheres with a Schultz Distribution)									
FW-HM [3]	377	331	373	360	485	449	378	429	274
Upper 95% Mean [nm]	1217	1107	795	1373	1165	1006	1146	796	1617
Lower 95% Mean [nm]	1164	1061	742	1323	1096	941	1093	733	1579
Coefficient of Variation	14%	13%	22%	12%	19%	21%	15%	26%	7%
Polydispersity, pd	0.173	0.159	0.267	0.326	0.251	0.348	0.391	0.513	0.682
Volume Fraction, ϕ x10^4		24.7 ±2.6	18.4 ±1.7	44.1±3.1	22.3±2.4	9.1±0.9	22.1 ±2.4	7.30 ±0.9	12.6 ±1.7
C. Small Microplastics, SMPs (USANS; polydisperse spheres with a Schultz Distribution)									
FW-HM [3]	N/A	N/A	2675 [4]	N/A	N/A	N/A	N/A	N/A	3680 [4]
Upper 95% Mean [nm]	N/A	N/A	7463	N/A	N/A	N/A	N/A	N/A	6753
Lower 95% Mean [nm]	N/A	N/A	7046	N/A	N/A	N/A	N/A	N/A	6414
Coefficient of Variation	N/A	N/A	7%	N/A	N/A	N/A	N/A	N/A	5%

[1] Model fits to data are depicted in (**Figs. 3 and S7**); [2] Structure factor was 1.0 unless noted otherwise; [3] Full width at half maximum of distribution, [4] Interference structure factor was employed, [5] not applicable (no data occurred at very low-*Q)*

3.4. Aggregation behavior of NPs suspended in 100% D_2O

Scattering contributions from both NPs and smaller-sized V particles can be observed when using 100% D_2O as solvent, in contrast to samples prepared under CMP conditions for V. Therefore, such a comparison will allow for differentiation between hetero- and homoaggregation involving NPs and V. Size-related parameters derived from the fitting of the lognormal and polydisperse sphere (Schultz distribution) models for SNPs and LNPs, respectively, and the average size and size distribution for the different combinations of NP and V concentrations are given in **Table 1 and Figs. 4 and S8**. For SNPs formed from suspensions of NPs (1%) +V, the same trend concerning stirring time was observed as per the CMP samples, that d_p decreased slightly (by ~5 nm); however, the average size was more than 2-fold smaller than observed at the CMP after 168 h of stirring and the size distribution was more monodisperse (**Figs. 4 and S8**). The results support the hypothesis noted above that SNPs in the presence of V for 1% NPs are composed of individual NPs, not aggregates, and demonstrate that particle dynamics between NPs and V differ between the two solvents, that SNPs are more susceptible to size reduction by convection and to interactions with V in 100% D_2O. Also, the size distribution of SNPs and LNPs narrowed as the *ex-situ* stirring time was increased **(Figs. 4 and S8)**.

For NPs (1%) in the absence of V and stirring, SMPs were ~2-fold larger for 100% D_2O compared to the CMP, and with an increase of stirring time, d_p for the former solvent decreased, approaching the same value as observed at the CMP, ~50 nm **(Fig. 4)**. An increase in stir time led to a similar trend for 5%NP+V (i.e., at a lower V/NP ratio), except that d_p was much larger initially, ~600 nm. The latter trend differs significantly from that observed at the CMP, indicating that SNPs more readily aggregate together in 100% D_2O. A similar trend exists for LNPs formed by NPs (1%) +V with increased *ex-situ* stirring time between solvents: a decrease of d_p, indicating that V induced size reduction in both solvents **(Fig. 4 C,D)**. A similar trend was observed for LNPs in the absence of V in 100% D_2O, in contrast to that observed at the CMP, indicating the propensity of LNPs to undergo size reduction to a greater extent in the former solvent **(Fig. 4D).** For a given stir time, the size of LNPs in 100% D_2O is similar between NPs in the absence and presence of V, but with sizes for NPs (1%) +V showing the greatest differences between solvents **(Fig. 4 C,D)**. This observation suggests that LNPs are mainly composed of PBAT and perhaps small amounts of nanoscale-sized V. The decrease of d_p for LNPs with stirring time for 5% NPs+V is consistent with 1% NPs in the presence and absence of V between 0 and 24 h, but the increase of size from 24 h to 168 h for LNPs and the major narrowing of the size distribution was not expected and may represent heteroaggregation between smaller V particles and LNPs **(Figs. 4D and S8F)**.

4 DISCUSSION

4.1. Effective NP concentration for samples measured using SANS and USANS

Although all suspended NP + V particles were dispersed well in the neutron beam through use of a tumbler cell as part of the sample environment, ϕ values determined from the model fitting of SANS oscillations for SNPs + LNPs, 0.0005-0.005, were well below the ~1% or 5% NP concentration levels of the samples by 3-4 orders of magnitude: **(Table S2)**. Therefore, we performed batch tests that replicated the conditions employed for the SANS and USANS samples, with centrifugation employed to remove excess NPs and V particles that were poorly retained in the suspension. Generally good agreement exists between ϕ values determined from the batch tests and via SANS and USANS in terms of order of magnitude, suggesting that only particles that were well suspended as a colloids in solution were measured by the latter method. However, ϕ values determined via SANS and USANS were in most cases higher than those determined through the batch tests because of the differences in sedimentation rates between the tumbling motion in the SANS and USANS sample cells for the former and centrifugation as employed for the latter. The level of agreement is greatest for the higher stir times and for the 1% NP + V conditions **(Table S2).** Trends for ϕ vs. NP and V concentrations and stir times determined by SANS generally agree with trends exhibited by the batch tests for samples employing CMP solvent but not for 100% D_2O **(Table S2 and Fig. 1)**. For the latter solvent, because of the smaller density difference between particles and solvent, suspensions are more sensitive to the differences in sedimentation rate that were described above.

4.2. Particles remaining in suspension are mostly NPs

Because of the ~2-fold higher density and the~300-fold higher size of V compared to NPs, the settling velocity of V is ~600,000-fold higher than for NP **(Table S3)**. Moreover, the particle size of V would need to be decreased 83-fold, to 458 nm, for its settling velocity to equal that of SNPs. Therefore, particles that remain well-suspended in solution are mainly NPs. In agreement, the size of small and large particles detected via SANS and USANS, respectively, are actually smaller (especially for the latter) for 1% NPs in the presence of V compared to the latter's absence, indicating no significant heteroaggregation occurred on the nanoscale **(Fig. 4)**. In agreement, batch tests for 0.5% V alone provided ϕ values that were lower than for NPs in the presence or absence of V, especially at higher stir times **(Table S2).** It is possible that V may contribute partly to the formation of SMPs. For example, after 168 h of stirring, the size of SMPs is slightly higher for 1% NP in the presence of V (~8000 nm)

compared to 5000-6000 for lower V/NP ratios in CMP solvent (1% NPs in the absence of V; 5% NP and 0.5% V; **Table 1**). However, SMPs in D_2O were detected only for 1% NPs and 5% NP / 0.5% V after 168 h (**Table 1**).

4.3. Do vermiculite and NPs form heteroaggregates?

The literature clearly shows that under conditions that mimic freshwater systems, negatively-charged minerals such as kaolinite and montmorillonite and PS-NPs do not undergo heteroaggregation during a short period (~0-2 h) due to electrostatic repulsion, in contrast to positively-charged minerals such as hematite and goethite that induce rapid heteroaggregation [41, 43, 44, 67]. However, a recent study found that heteroaggregation between PS and polyvinyl chloride (PVC)-NPs and silica nanoparticles (each of size ~250 nm) occurred in the presence of $CaCl_2$ at ≥0.1 mM [38]. Another study detected heteroaggregation between PE-MPs and negatively-charged clay minerals (both particles of size ~ 10 μm), but only in the presence of >100 mM NaCl [68]. Electrostatic repulsion occurs for the systems investigated herein, noted by zeta potential values of -20 to -30 mV for NPs [51] and -8 to -13 mV for V **(Fig. S9)** in the complete absence of salts, the latter in agreement with the literature [69]. Therefore, heteroaggregation on a short time scale is unlikely.

However, the decrease of ϕ with stir time for SNPs in the presence of V, especially for 1% NPs + V (i.e., the largest V/NP ratio) in CMP solvent, conditions where homoaggregation of NPs did not occur, may be due to heteroaggregation, with NPs that were suspended in solution being removed due to adsorption to V microparticles. Moreover, smaller-sized particles are more likely to undergo aggregation because of their higher surface area and colloidal behavior. In contrast, ϕ increased with stir time for NP in the absence of V for CMP solvent **(Table 1)**. The mechanism for binding is unclear but may be due to ion pairing between the NPs and cations such as Mg^{2+} that are located on the edges of V [70]. A similar explanation was proposed for the observed heteroaggregation of PS-NPs and montmorillonite [36]. Alternatively, hydrophobic interactions and available surface area have been proposed as driving forces for aggregation of MPs and negatively-charged riverine sediment [71]. Generally, heteroaggregates within the size range probed by SANS were not observed; however, as mentioned previously, the increase of size from 24 h to 168 h of stir time for LNPs in 100% D_2O, i.e., under conditions where V is not contrast matched out, may represent heteroaggregation between smaller V particles and LNPs.

4.4. Vermiculite promotes size reduction of LNPs

The most significant finding from this study is that V promoted the reduction of d_p for LNPs in particular and SNPs to a smaller extent, the extent of which increased with stir time and an increase of the V/NP ratio **(Fig. 4)**. This finding has not been reported previously. Most of the previous studies on NP aggregation behavior employed monodisperse spherical, mainly PS-, NPs, focused on short-time frames, and employed concentrations typically below 100 ppm (reviewed in [26]). The current study employed NPs prepared from biodegradable mulch films that are bimodal in size distribution, composed of LNP and SNP subpopulations, and are irregularly-shaped [51]. PBAT-NPs, particularly LNPs, were susceptible to size reduction in the presence of shear, as observed during wet grinding [51]. Concentrations of NPs and soil mineral particles employed herein are several-fold higher than employed in previous studies in the literature [26]. It is evident that the collisions between V and NPs at the concentrations employed herein, for which the majority of V particles remain free during the 168 d period where the particles were stirred. This result suggests that LNPs residing near the soil-freshwater surface within the vadose zone are likely to undergo size reduction to SNPs when in the presence of suspended silt particles and convective flow of streams or flooding rain.

4.5. Limitations of SANS and USANS analysis for studying NP-related dynamics

SANS and USANS analyses serve as a powerful tool for analysis of NP dynamics due to their ability to measure nanoscale suspensions *in situ* (through use of the tumbler cell), thereby minimizing the induction of artifacts in the results associated with complex sample preparations, and the employment of neutron contrast matching to isolate particular components of systems in the neutron beam through selective deuteration. In this paper, analysis of NP dynamics for suspensions of NP/V mixtures was achieved for suspensions formed in 67% D_2O/33% H_2O, the contrast match point for V, which minimized the SANS and USANS signal for V. In addition, neutrons are non-invasive and will not promote damage to solution components.

However, there are several limitations for using the SANS/USANS approach. First, there likely exists a practical minimum for the concentration of particles that can be used, because as the concentration of particles is decreased, the exposure time to neutrons required to achieve high quality data will increase. In addition, particles of size larger than ~10 μm cannot be resolved using SANS/USANS. In our case, the largest sized particles observable were SMPs of size ~8000 nm (Table 1). Furthermore, the difference in density between solvents of different deuteration levels affected the interpretation of results for particle dynamics. For example, the difference complicated comparing results between the two solvents employed for SANS/USANS. Neat D_2O is denser and less effective in the solvation of

surface functional groups for V and NPs compared to CMP solvent or H_2O [72], thereby enhancing the homoaggregation of SNPs suspended in D_2O. The settling velocity of NPs is 25% lower in D_2O, thereby enhancing the propensity of SNPs to aggregate **(Table S3)**. In agreement, SNPs underwent homoaggregation, observed by the ≥2-fold larger size for NPs in the absence of stirring, for 1% NPs and 5% NPs + V **(Fig. 4)**. Consistent with these results is the higher concentration of NPs suspended in solution for 100% D_2O in the batch tests **(Fig. 1)**. Although homoaggregation generally does not occur in freshwater in a short time period (~< 12 h), a recent study detected homoaggregation of PS NPs in lake and river water over longer periods of time (12-72 h) at 30°C due to partial neutralization of the NPs' negative charge through adsorption of NOM and increased temperature [56].

The settling velocity for V microparticles is also lower in D_2O compared to CMP solvent, but to a much lesser extent, 9.2% **(Table S3)**, in agreement with the higher V concentration occurring in the former solvent **(Fig. 1)**. The increased retention time of V microparticles suspended in solution likely led to the reduced size of SNPs in D_2O compared to CMP solvent for the 1% NP+V treatment **(Table S3)**. Similarly, heteroaggregation between SiO_2 nanoparticles and PS-NPs was greater than for SiO_2 and PVC-NPs because the latter NPs were denser than the former and therefore were more prone to settle out of solution [38]. By the same token, the differences in solvent density and polarity between D_2O and H_2O lead to differences in NP and V settling velocities between the solvents **(Table S3)**, hence complicating the relatability of findings obtained via SANS/USANS to observed dynamics in ecosystems.

5 CONCLUSIONS

This study focused on deepening the understanding of particle dynamics of NPs dispersed in water in the presence of soil (V) microparticles, simulating the environment existing at soil-water interfaces in the vadose zone of agroecosystems. SANS, USANS, and the neutron contrast matching technique allowed for the *in situ* analysis of NPs by employing light tumbling of the suspensions in the neutron beam, with interference from V minimized. The original NPs, derived from a pristine BDM composed mainly of the biodegradable polyester PBAT and prepared using a protocol that simulates the slow degradative process that would occur over time in soils [51], consists of two subpopulations of SNPs (<200 nm) and LNPs (500-1200 nm). We found that the SNPs were composed of individual particles that underwent homoaggregation when present at 5% but not 1%. Exposure to convective stirring for 1% NP led to a slight decrease in size and a narrowing of the size distribution (greater in the presence of V), with the larger SNPs selectively undergoing size reduction. In the absence of V, ϕ for SNPs

increased with stirring, while the opposite trend occurred in the presence of V, which likely resulted from aggregation of SNPs with V microparticles. Adding V to a 1% NP suspension led to a 2-fold decrease in size for LNPs when exposed to 168 h of stirring.

In comparison, the size and volume fraction of LNPs derived from films did not change appreciably in the absence of V. Similar trends occurred when V was added to a 5% NP suspension, but with the decrease of size for LNPs occurring after 24 h of stirring rather than steadily across the 168-h stirring cycle for 1% NPs. Employing 100% D_2O as a solvent for SANS and USANS allowed us to better observe V nanoparticles. From comparing data obtained using the two solvents, most of the particles consisted of individual SNPs and LNPs without V. However, a direct comparison of results between the solvents was not always possible because particle dynamics differed between the two solvents, with SNPs being more prone to aggregate in 100% D_2O and exist at a smaller size. Therefore, one must consider this difference when planning and evaluating SANS and USANS experiments employing different deuteration levels in solvents.

The results demonstrate that LNPs are more fragile than SNPs and are more likely to undergo size reduction (thereby forming SNPs) when exposed to soil microparticles under convection. In contrast, SNPs undergo size reduction to a minor extent during convection, although they form homoaggregates as their concentration is increased in the absence of V, and they interact with V microparticles with increased convection. Therefore, the behavior of NPs near water-soil interfaces is complex, with NP size and the presence of convective forces being critical factors controlling the dynamics.

DECLARATION OF COMPETING INTEREST

The authors declare that they have no known competing financial interests or personal relationships that could have appeared to influence the work reported in this paper.

ACKNOWLEDGMENTS

The initial feedstocks for preparing M/NPs of PBAT-based biodegradable mulch film were kindly provided by BioBag Americas, Inc. (Dunevin, FL, USA).

FUNDING

The authors gratefully acknowledge the financial support provided through the USDA (Grant 2020-67019-31167), UTIA SPRINT Program, the Herbert College of Agriculture, the Biosystems

Engineering and Soil Department, and the Science Alliance at the University of Tennessee, Knoxville, TN, for this research. Measurements on Bio-SANS that is part of the Center for Structural Molecular Biology funded by DOE OBER project ERKP291. A portion of this research used resources at the High Flux Isotope Reactor and Spallation Neutron Source, a DOE Office of Science User Facility operated by the Oak Ridge National Laboratory. The beam time was allocated to Bio-SANS on proposal number IPTS-22148.1 and USANS on proposal number IPTS-28744.1.

CRediT authorship contribution statement

Hayes, Astner, O'Neill, and Evans obtained the financial resources necessary to complete the research work in this paper at the University of Tennessee, while Pingali, Urban, and Littrell obtained funding for neutron scattering experiments at ORNL. Astner, Hayes, O'Neill, and Pingali designed and performed the experiments described in this manuscript, while all authors contributed to the overall project that led to the specific study described herein. Hayes is the project lead and the supervisor for Astner. Astner and Hayes performed the analysis and interpretation of the data. Astner and Hayes wrote the first draft of this manuscript, while all authors contributed to the revision of this draft.

Conflict-of-Interest Statement

There are no conflicts to declare

Data Availability Statement:

Data is available at: https://doi.org/10.5061/dryad.2z34tmpws

REFERENCES

1. Y.-B. Ma, Z.-Y. Xie, N. Hamid, Q.-P. Tang, J.-Y. Deng, L. Luo and D.-S. Pei, Recent advances in micro (nano) plastics in the environment: Distribution, health risks, challenges and future prospects, *Aquatic Toxicology*, 2023, 106597.

2. V. Kumar, E. Singh, S. Singh, A. Pandey and P. C. Bhargava, Micro-and nano-plastics (MNPs) as emerging pollutant in ground water: Environmental impact, potential risks, limitations and way forward towards sustainable management, *Chemical Engineering Journal*, 2023, **459**, 141568.

3. S. Selonen, A. Dolar, A. J. Kokalj, T. Skalar, L. P. Dolcet, R. Hurley and C. A. van Gestel, Exploring the impacts of plastics in soil–The effects of polyester textile fibers on soil invertebrates, *Science of the Total Environment*, 2020, **700**, 134451.

4. E. Lahive, R. Cross, A. I. Saarloos, A. A. Horton, C. Svendsen, R. Hufenus and D. M. Mitrano, Earthworms ingest microplastic fibres and nanoplastics with effects on egestion rate and long-term retention, *Science of the Total Environment*, 2022, **807**, 151022.

5. O. Bansal and A. Singh, A review on microplastic in the soils and their impact on soil microbes, crops and humans, *International Journal of Research*, 2022, **10**, 245-273.

6. D. Ghosh, P. Ghorai, S. Sarkar, K. S. Maiti, S. R. Hansda and P. Das, Microbial assemblage for solid waste bioremediation and valorization with an essence of bioengineering, *Environmental Science and Pollution Research*, 2023, **30**, 16797-16816.

7. V.-R. Le, M.-K. Nguyen, H.-L. Nguyen, C. Lin, M. R. J. Rakib, V.-A. Thai, V.-G. Le, G. Malafaia and A. M. Idris, Organic composts as A vehicle for the entry of microplastics into the environment: A comprehensive review, *Science of The Total Environment*, 2023, 164758.

8. S. Maity, R. Guchhait, M. B. Sarkar and K. Pramanick, Occurrence and distribution of micro/nanoplastics in soils and their phytotoxic effects: A review, *Plant, Cell & Environment*, 2022, **45**, 1011-1028.

9. A. F. Astner, A. B. Gillmore, Y. Yu, M. Flury, J. M. DeBruyn, S. M. Schaeffer and D. G. Hayes, Formation, behavior, properties and impact of micro-and nanoplastics on agricultural soil ecosystems (A Review), *NanoImpact*, 2023, 100474.

10. M. C. Rillig, A. Abel de Souza Machado, A. Lehmann and U. Kluemper, Evolutionary implications of microplastics for soil biota, *Environ. Chem.*, 2019, **16**, 3-7.

11. M. C. Rillig, Microplastic in terrestrial ecosystems and the soil? , *Soil Biology and Biochemistry*, 2012, **45**, 123-130.

12. S. Zhao, M. C. Rillig, H. Bing, Q. Cui, T. Qiu, Y. Cui, J. Penuelas, B. Liu, S. Bian, F. A. Monikh, J. Chen and L. Fang, Microplastic pollution promotes soil respiration: A global-scale meta-analysis, *Global Change Biology*, 2024, **30**, e17415.

13. C. J. Beloe, M. A. Browne and E. L. Johnston, Plastic Debris As a Vector for Bacterial Disease: An Interdisciplinary Systematic Review, *Environmental Science & Technology*, 2022, **56**, 2950-2958.

14. F. Huang, J. Hu, L. Chen, Z. Wang, S. Sun, W. Zhang, H. Jiang, Y. Luo, L. Wang, Y. Zeng and L. Fang, Microplastics may increase the environmental risks of Cd via promoting Cd uptake by plants: A meta-analysis, *Journal of Hazardous Materials*, 2023, **448**, 130887.

15. R. R. Hurley and L. Nizzetto, Fate and occurrence of micro (nano) plastics in soils: Knowledge gaps and possible risks, *Current Opinion in Environmental Science & Health*, 2018, **1**, 6-11.

16. H. Yu, M. Liu, D. Gang, J. Peng, C. Hu and J. Qu, Polyethylene microplastics interfere with the nutrient cycle in water-plant-sediment systems, *Water Research*, 2022, **214**, 118191.

17. T. Li, L. Cui, Z. Xu, H. Liu, X. Cui and P. Fantke, Micro-and nanoplastics in soil: Linking sources to damage on soil ecosystem services in life cycle assessment, *Science of the Total Environment*, 2023, 166925.

18. C. Moeck, G. Davies, S. Krause and U. Schneidewind, Microplastics and nanoplastics in agriculture—A potential source of soil and groundwater contamination?, *Grundwasser*, 2023, **28**, 23-35.

19. S. Ray and S. T. Shaju, Bioaccumulation of Pesticides in Fish Resulting Toxicities in Human Through Food Chain and Forensic Aspects, *Journal of Survey in Fisheries Sciences*, 2023, **38**, 2223-2242.

20. G. Kibria, Impacts of microplastic on fisheries and seafood security—global analysis and synthesis, *Science of The Total Environment*, 2023, 166652.

21. O. Latchere, I. Métais, H. Perrein-Ettajani, M. Lemoing, A. Feurtet-Mazel, P. Gonzalez, G. Daffe, J. Gigault, C. Catrouillet, A. Châtel and M. Baudrimont, Trophic transfer effects of PS nanoplastics and field-derived nanoplastics in the freshwater clam Corbicula fluminea, *Aquatic Toxicology*, 2024, **277**, 107160.

22. G. Kishore, B. M. Babu and L. D. Mattaparti, Influence of plastic mulching and irrigation levels on soil temperature, moisture and water use efficiency of tomato crop (Solanum lycopersicum), *International Journal of Plant & Soil Science*, 2022, **34**, 277-282.

23. S. Kasirajan and M. Ngouajio, Polyethylene and biodegradable mulches for agricultural applications: a review, *Agronomy for Sustainable Development*, 2012, **32**, 501-529.

24. Z. Mansoor, F. Tchuenbou-Magaia, M. Kowalczuk, G. Adamus, G. Manning, M. Parati, I. Radecka and H. Khan, Polymers Use as Mulch Films in Agriculture—A Review of History, Problems and Current Trends, *Polymers*, 2022, **14**, 5062.

25. D. Griffin-LaHue, S. Ghimire, Y. Yu, E. J. Scheenstra, C. A. Miles and M. Flury, In-field degradation of soil-biodegradable plastic mulch films in a Mediterranean climate, *Science of The Total Environment*, 2022, **806**, 150238.

26. S. Reynaud, A. Aynard, B. Grassl and J. Gigault, Nanoplastics: From model materials to colloidal fate, *Current Opinion in Colloid & Interface Science*, 2022, **57**, 101528.

27. Y. Liu, Y. Ben, R. Che, C. Peng, J. Li and F. Wang, Uptake, transport and accumulation of micro-and nano-plastics in terrestrial plants and health risk associated with their transfer to food chain-A mini review, *Science of The Total Environment*, 2023, 166045.

28. Y. Liang, X. Cao, A. Mo, J. Jiang, Y. Zhang, W. Gao and D. He, Micro (nano) plastics in plant-derived food: Source, contamination pathways and human exposure risks, *TrAC Trends in Analytical Chemistry*, 2023, 117138.

29. Y. Liu, R. Guo, S. Zhang, Y. Sun and F. Wang, Uptake and translocation of nano/microplastics by rice seedlings: Evidence from a hydroponic experiment, *Journal of Hazardous Materials*, 2022, **421**, 126700.

30. W. Wang, A. T. N. Do and J.-H. Kwon, Ecotoxicological effects of micro-and nanoplastics on terrestrial food web from plants to human beings, *Science of The Total Environment*, 2022, **834**, 155333.

31. N. U. Benson, O. D. Agboola, O. H. Fred-Ahmadu, G. E. De-la-Torre, A. Oluwalana and A. B. Williams, Micro (nano) plastics prevalence, food web interactions, and toxicity assessment in aquatic organisms: a review, *Frontiers in Marine Science*, 2022, **9**, 851281.

32. Q. Wang, J. Bai, B. Ning, L. Fan, T. Sun, Y. Fang, J. Wu, S. Li, C. Duan and Y. Zhang, Effects of bisphenol A and nanoscale and microscale polystyrene plastic exposure on particle uptake and toxicity in human Caco-2 cells, *Chemosphere*, 2020, **254**, 126788.

33. S. W. Kim and Y.-J. An, Edible size of polyethylene microplastics and their effects on springtail behavior, *Environ. Pollut. (Oxford, U. K.)*, 2020, **266**, 115255.

34. C. Schwaferts, R. Niessner, M. Elsner and N. P. Ivleva, Methods for the analysis of submicrometer- and nanoplastic particles in the environment, *TrAC Trends in Analytical Chemistry*, 2019, **112**, 52-65.

35. C. Chinglenthoiba, K. T. T. Amesho, D. G. C. V. Reddy, S. Chellappan and M. N. Lani, Microplastic as an Emerging Environmental Threat: A Critical Review on Sampling and Identification Techniques Focusing on Aquactic Ecoystem, *Journal of Polymers and the Environment*, 2023, **31**, 1725-1747.

36. N. Singh, E. Tiwari, N. Khandelwal and G. K. Darbha, Understanding the stability of nanoplastics in aqueous environments: effect of ionic strength, temperature, dissolved organic matter, clay, and heavy metals, *Environmental Science: Nano*, 2019, **6**, 2968-2976.

37. Z. Song, X. Yang, F. Chen, F. Zhao, Y. Zhao, L. Ruan, Y. Wang and Y. Yang, Fate and transport of nanoplastics in complex natural aquifer media: Effect of particle size and surface functionalization, *Science of The Total Environment*, 2019, **669**, 120-128.

38. F. Abdolahpur Monikh, J. T. K. Quik, M. R. Wiesner, A. Tapparo, P. Pastore, H.-P. Grossart, J. Akkanen, R. Kortet and J. V. K. Kukkonen, Importance of Attachment Efficiency in Determining the Fate of PS and PVC Nanoplastic Heteroaggregation with

Natural Colloids Using a Multimedia Model, *Environmental Science & Technology*, 2025, **59**, 4674-4683.

39. S. Dong, W. Cai, J. Xia, L. Sheng, W. Wang and H. Liu, Aggregation kinetics of fragmental PET nanoplastics in aqueous environment: Complex roles of electrolytes, pH and humic acid, *Environmental Pollution*, 2021, **268**, 115828.

40. F. Zhang, Z. Wang, S. Wang, H. Fang and D. Wang, Aquatic behavior and toxicity of polystyrene nanoplastic particles with different functional groups: Complex roles of pH, dissolved organic carbon and divalent cations, *Chemosphere*, 2019, **228**, 195-203.

41. X. Zhou, A. Li, M. Cerne, S. MacRae, I. Eggleston, H. Qiao, X. Li, G. Huang, P. Wang, J. Zhao and B. Xing, Nanoplastic-mineral heteroaggregation under varying degrees of plastic pollution: Implications for antibiotic adsorption in aquatic systems, *Chemical Engineering Journal*, 2025, **503**, 158444.

42. O. Oriekhova and S. Stoll, Heteroaggregation of nanoplastic particles in the presence of inorganic colloids and natural organic matter, *Environmental Science: Nano*, 2018, **5**, 792-799.

43. Y. Zhang, Y. Luo, X. Guo, T. Xia, T. Wang, H. Jia and L. Zhu, Charge mediated interaction of polystyrene nanoplastic (PSNP) with minerals in aqueous phase, *Water Research*, 2020, **178**, 115861.

44. R. Xie, X. Xing, X. Nie, X. Ma, Q. Wan, Q. Chen, Z. Li and J. Wang, Deposition behaviors of carboxyl-modified polystyrene nanoplastics with goethite in aquatic environment: Effects of solution chemistry and organic macromolecules, *Science of The Total Environment*, 2023, **904**, 166783.

45. A. F. Astner, D. G. Hayes, S. V. Pingali, H. M. O'Neill, K. C. Littrell, B. R. Evans and V. S. Urban, Effects of soil particles and convective transport on dispersion and aggregation of nanoplastics via small-angle neutron scattering (SANS) and ultra SANS (USANS), *PLoS One*, 2020, **15**, e0235893.

46. S. Gündoğdu, F.-C. Mihai, E. K. Fischer, M. C. Blettler, O. C. Turgay, M. O. Akça, B. Aydoğan and B. Ayat, Micro and nano plastics in groundwater systems: A review of current knowledge and future perspectives, *TrAC Trends in Analytical Chemistry*, 2023, **165**, 117119.

47. C. Veclin, C. Desmet, A. Pradel, A. Valsesia, J. Ponti, H. El Hadri, T. Maupas, V. Pellerin, J. Gigault, B. Grassl and S. Reynaud, Effect of the Surface Hydrophobicity–Morphology–Functionality of Nanoplastics on Their Homoaggregation in Seawater, *ACS ES&T Water*, 2022, **2**, 88-95.

48. M. B. Anunciado, D. G. Hayes, L. C. Wadsworth, M. E. English, S. M. Schaeffer, H. Y. Sintim and M. Flury, Impact of agricultural weathering on physicochemical properties of biodegradable plastic mulch films: Comparison of two diverse climates over four successive years, *Journal of Polymers and the Environment*, 2021, **29**, 1-16.

49. A. Astner, D. Hayes, H. O'Neill, B. Evans, S. Pingali, V. Urban and T. Young, Mechanical formation of micro-and nano-plastic materials for environmental studies in agricultural ecosystems, *Science of The Total Environment*, 2019, **685**, 1097-1106.

50. A. F. Astner, D. G. Hayes, H. M. O'Neill, B. R. Evans, S. V. Pingali, V. S. Urban and T. M. Young, Forming Micro-and Nano-Plastics from Agricultural Plastic Films for Employment in Fundamental Research Studies, *Journal of Visualized Experiments: Jove*, 2022, **185**, e64112.

51. A. Astner, D. Hayes, H. O'Neill, B. Evans, S. Pingali, V. Urban, S. Schaeffer and T. Young, Assessment of cryogenic pretreatment for simulating environmental weathering in the formation of surrogate micro-and nanoplastics from agricultural mulch film, *Science of The Total Environment*, 2023, **870**, 161867.

52. C. A. Schneider, W. S. Rasband and K. W. Eliceiri, NIH Image to ImageJ: 25 years of image analysis, *Nature Methods*, 2012, **9**, 671-675.

53. International Organization for Standardization (ISO), *Geotechnical investigation and testing; Identification and classification of soil. Part 1: Identification and description (ISO 14688-1:2017)*, ISO, Geneva, Switzerland, 2017.

54. L. C. van Rijn, *Principles of Sediment Transport in Rivers, Estuaries and Coastal Seas*, Aqua Publications, Amsterdam, 1993.

55. J. Robotham, G. Old, P. Rameshwaran, D. Sear, D. Gasca-Tucker, J. Bishop, J. Old and D. McKnight, Sediment and Nutrient Retention in Ponds on an Agricultural Stream: Evaluating Effectiveness for Diffuse Pollution Mitigation, *Water*, 2021, **13**, 1640.

56. K. Ko and H. Chung, Colloidal stability of UV-aged and protein-coated nanoplastics in natural waters under warming, *Environmental Pollution*, 2025, **368**, 125772.

57. K. Tallec, O. Blard, C. González-Fernández, G. Brotons, M. Berchel, P. Soudant, A. Huvet and I. Paul-Pont, Surface functionalization determines behavior of nanoplastic solutions in model aquatic environments, *Chemosphere*, 2019, **225**, 639-646.

58. M. Agamalian, L. Heroux, K. Littrell and J. Carpenter, Paris, France, 2018.

59. W. T. Heller, M. Cuneo, L. Debeer-Schmitt, C. Do, L. He, L. Heroux, K. Littrell, S. V. Pingali, S. Qian and C. Stanley, The suite of small-angle neutron scattering instruments at Oak Ridge National Laboratory, *Journal of Applied Crystallography*, 2018, **51**, 242-248.

60. W. T. Heller, V. S. Urban, G. W. Lynn, K. L. Weiss, H. M. O'Neill, S. V. Pingali, S. Qian, K. C. Littrell, Y. B. Melnichenko and M. V. Buchanan, The Bio-SANS instrument at the high flux isotope reactor of Oak Ridge National Laboratory, *Journal of Applied Crystallography*, 2014, **47**, 1238-1246.

61. S. R. Kline, Reduction and analysis of SANS and USANS data using IGOR Pro, *Journal of Applied Crystallography*, 2006, **39**, 895-900.

62. J. Ilavsky and P. R. Jemian, Irena: tool suite for modeling and analysis of small-angle scattering, *Journal of Applied Crystallography*, 2009, **42**, 347-353.

63. P. W. Schmidt, Small-angle scattering studies of disordered, porous and fractal systems, *Journal of Applied Crystallography*, 1991, **24**, 414-435.

64. M. Kotlarchyk and S. H. Chen, Analysis of small angle neutron scattering spectra from polydisperse interacting colloids, *The Journal of Chemical Physics*, 1983, **79**, 2461-2469.

65. B. H. Zimm, The scattering of light and the radial distribution function of high polymer solutions, *The Journal of Chemical Physics*, 1948, **16**, 1093-1099.

66. G. Beaucage, Approximations leading to a unified exponential/power-law approach to small-angle scattering, *Journal of Applied Crystallography*, 1995, **28**, 717-728.

67. N. Liu, Y. Kong, X. Cao, L. Yue, Z. Wang and X. Li, Both nanoplastic and iron mineral types determine their heteroaggregation: Aggregation kinetics and interface process, *Journal of Hazardous Materials*, 2024, **470**, 134192.

68. Y. Wang, X. Chen, F. Wang and N. Cheng, Influence of typical clay minerals on aggregation and settling of pristine and aged polyethylene microplastics, *Environmental Pollution*, 2023, **316**, 120649.

69. H. Sis and T. Uysal, Removal of heavy metal ions from aqueous medium using Kuluncak (Malatya) vermiculites and effect of precipitation on removal, *Applied Clay Science*, 2014, **95**, 1-8.

70. S. İşçi, Intercalation of vermiculite in presence of surfactants, *Applied Clay Science*, 2017, **146**, 7-13.

71. J. L. Stead and T. Bond, The impact of riverine particles on the vertical velocities of large microplastics, *Science of The Total Environment*, 2023, **896**, 165339.

72. G. Giubertoni, M. Bonn and S. Woutersen, D_2O as an Imperfect Replacement for H_2O: Problem or Opportunity for Protein Research?, *The Journal of Physical Chemistry B*, 2023, **127**, 8086-8094.

Data Availability Statement:

Data is available at: https://doi.org/10.5061/dryad.2z34tmpws